Akademeia (2011) **1**(1): ea0105

Physical Sciences
ARTICLE

Structural single Crystal, ^{23}Na and ^{31}P MAS NMR and conductivity studies of $Na_2HPO_4NaH_2PO_4Te(OH)_6$

Hatem Derbel [a‡], **Saber Kamoun** [a], **Faouzi Hlel** [a], **Mohamed Gargouri** [a]

[a] *Laboratoire de l'état Solide, Faculté des Sciences de Sfax, BP 802, 3018 Sfax, Tunisia*

Single crystal X-ray diffractometry of the sodium phosphate tellurate compound $Na_2HPO_4NaH_2PO_4Te(OH)_6$ (NaPTe) shows that the compound crystallizes in a trigonal system with a P3 space group. The unit cell parameters were as follows: a = 7.861(1) Å and c = 10.8326(1) Å, V = 579.7(2) Å^3 and Z = 2. The asymmetric unit is made up of two unequivalent $Te(OH)_6$ groups, four unequivalent PO_4 groups and two unequivalent Na^+ cations. Material cohesion is built of O-H···O bondings and ionic interactions. Magic angle spinning nuclear magnetic resonance (MAS NMR) ^{31}P and ^{23}Na analysis were used to confirm the crystal structure investigation. Indeed, the observed values of ^{23}Na NMR chemical shift are found to be -4.58 and 3.35 ppm revealing the presence of two non-equivalent sodium nuclei in the structure. Moreover, the simulation of the ^{31}P NMR spectrum exhibits four sites with a similar abundance observed at 1.6, 3.8, 3.2 and 2.8 ppm chemical shifts. AC complex impedance measurements performed on the NaPTe compound showed a significant level of conductivity at high temperatures, probably attributable to the motion of Na^+ ions and H^+ protons. The conduction process in the AC conductivity is explained by the large overlapping polaron model up to 100°C.

KEYWORDS: NaPTe material, crystal structure, ^{31}P and ^{23}Na MAS NMR, conductivity

Telluric acid can form stable adducts with a large variety of organic and inorganic compounds of considerable importance due to the fact that the $Te(OH)_6$ moiety acts as both acceptor and donor of hydrogen bonds. Structures of compounds with the general formula $M_2AO_4Te(OH)_6$ (where M is a monovalent cation, Na, K, Rb, Cs, NH_4 and A is S, Se) have been reported [1, 2, 3, 4, 5].

These compounds have attracted much attention for their structural phase transitions and their associated physical properties: ferroelectricity, dielectric relaxation and especially a phase transition into a state characterized by a high protonic conductivity [6, 7, 8, 9]. KH_2PO_4 appears to be one of the most conductive compounds in a family of acid salts of alkaline metals. The solid acid salts with the general formula $M_xH_y(PO_4)$ (M=Cs, Rb, K, Na, Li, NH_4) [10, 11, 12, 13, 14] undergo a superionic phase transition at 50–230°C accompanied by a increase of conductivity. The superionic phases exhibit general features due to the existence of a disordered hydrogen bond network.

[‡] Correspondence: derbel.hatem@lycos.com

Received: October 02, 2010; **Accepted:** March 14, 2011

The influence of anionic substitution on crystal symmetry has been reported in previous studies. In fact, while $Rb_2HPO_4RbH_2PO_4Te(OH)_6$ [15], $Cs_2HPO_42CsH_2PO_4Te(OH)_6$ [16], $Tl_2HPO_42TlH_2PO_4Te(OH)_6$ [17] and $(NH_4)_2HPO_42(NH_4)H_2PO_4Te(OH)_6$ [18] crystallise in the monoclinic, with the respective space groups $P2_1/a$, $P2_1/m$, Cm and Pn, the sodium phosphate tellurate $Na_2HPO_4NaH_2PO_4Te(OH)_6$ exhibits the $P6_322$ space group [19].

In all cases, the crystal structure determination shows that the main feature of these atomic arrangements is the coexistence of both the TeO_6 octahedra and PO_4 tetrahedra as independent units.

For all their importance the aforementioned studies on the phosphate tellurate family have never examined their basic physical properties. The study of such properties was the original aim of our research. Surprisingly, our preparation of $Na_2HPO_4NaH_2PO_4Te(OH)_6$ as described by Pouchot [19] resulted in a compound with a different structure. This drove us to reinvestigate its detailed structure with X ray crystallography, ^{23}Na and ^{31}P MAS NMR, and impedance spectroscopy.

Materials/Methods

Preparation of $Na_2HPO_4NaH_2PO_4Te(OH)_6$

The title compound $Na_2HPO_4NaH_2PO_4Te(OH)_6$ is synthesized by slow evaporation at room temperature of an aqueous solution of the telluric acid (H_6TeO_6), the sodium carbonate (Na_2CO_3) and the phosphoric acid (H_3PO_4) mixed in molar proportions 1:3:4. Schematically the reaction is:

$$3/2\ Na_2CO_3 + 2\ H_3PO_4 + H_6TeO_6 \longrightarrow Na_2HPO_4NaH_2PO_4Te(OH)_6 + 3/2(CO_2 + H_2O)$$

After approximately ten days, colourless hexagonal crystals appeared in the solution.

Solid State MAS NMR Measurements

The solid-state ^{23}Na and ^{31}P MAS NMR spectra at 300 K were recorded on a powdered sample with a Bruker WB 300 FT- MAS NMR spectrometer operating at 79.39 MHz for the ^{23}Na nucleus and 121.5 MHz for the ^{31}P nucleus. Spectra were recorded using single pulse field of 10 kHz at 7.05 T.

The ^{23}Na and ^{31}P chemical shifts are reported relative to an aqueous (1 M) NaCl solution and 85% H_3PO_4, respectively. The acquisition parameters for ^{23}Na nuclei are as follows; a 15.6 μs pulse length, a 1 s pulse delays and 1024 scans. The ^{31}P MAS NMR spectrum is obtained with a 15.75 μs pulse duration, a pulse delay of 1 s and with 4096 scans. The simulations of the isotropic bands and of the spinning sideband manifolds were performed using the Dmfit program [20]. For the ^{23}Na MAS NMR spectrum, the program considers the average Hamiltonian for the second order quadripolar interaction and includes intensities measured from the centerband as well as the spinning sidebands from the isotropic bands.

Crystal structure study

A single crystal (0.42mm x 0.43mm x 0.24mm) was selected by optical examination. X-ray crystallography was carried out using the Stoe Image Plate Diffraction System and the Siemens SMART CCD area-detector diffractometer with a graphite monochromated Mo K_α radiation (0.71073 Å). The empirical absorption corrections were applied using SADABS data reflections [21]. The structure reported by Averbuch-Pouchot [19] was in a hexagonal system with a $P6_322$ space group. The extinction rule in the $P6_322$ space group exhibits the absence of any 00l (l=2n) reflections and uses only 685 reflections in the 2θ range (3-30°). In our study, confirmed by localization of two Na sites and four P sites by NMR-MAS, we have increased the 2θ range

Table 1: Main crystallographic and refinement data for $Na_2HPO_4NaH_2PO_4Te(OH)_6$

Formula	$Na_2HPO_4.NaH_2PO_4.Te(OH)_6$
Formula weight ($g.mol^{-1}$)	489.57
Color	Colourless
Shape	Bipyramid hexagonal
Crystal dimensions (mm^3)	0.24x0.23x0.14
Crystal system	trigonal
Space group	P3
Cell parameters	
a (Å)	7.861 (1)
c (Å)	10.8326 (1)
V ($Å^3$)	579.7 (2)
Z	2
$\theta_{min}/\theta_{max}$ (°)	4.81/43.98
Intensity measurements	
Temperature (K)	293(2)
Diffractometer	Graphite plate
λ (Mo K_α) (Å)	0.71069
$-15 \leq h \leq 12$	
$-4 \leq k \leq 14$	
$-21 \leq l \leq 20$	
ρ (g/cm^3)	2.805
Reflections collected / unique	12247/5055 (Rint = 0.0239)
Structure determination	
Absorption correction	SADABS
Structure resolution	Patterson methods (SHELX-S 86)
Structure refinement with	SHELX-L 93
Reflections with $Fo>2\sigma(Fo)$	4822
Refinement	F^2 full matrix
Refined parameters	122
Goodness of fit	1.355
Final R and Rw	0.0258, 0.0601
Final R and Rw for all data	0.027, 0.0611
Largest feature diff. map	1.922, -4.775 $Å^{-3}$

$w = 1/[\sigma^2 (Fo)^2 + (0.028\ P)^2 + 0\ P]$ where $P = [Fo^2 + 2\ Fc^2]/3$

Table 2. Main geometrical features, bond distances, angles and ID Baur Distortion.

Na(1)O$_6$

Na1	O4	O11	O8^{iii}	O1^{iii}	O3^{i}	O9^{viii}
O4	**2.364(2)**	75.18(4)	157.94(5)	88.09(5)	80.98(4)	109.95(4)
O11	2.885(2)	**2.364(2)**	88.11(5)	157.88(5)	88.09(5)	80.95(4)
O8^{iii}	4.679(2)	3.315(1)	**2.403(1)**	111.37(3)	91.64(4)	80.81(4)
O1^{iii}	3.314(3)	4.679(1)	3.969(2)	**2.403(1)**	80.81(4)	91.58(4)
O3^{i}	3.218(7)	4.058(1)	3.580(0)	3.237(1)	**2.586(1)**	166.61(4)
O9^{viii}	4.056(3)	3.218(1)	3.237(1)	3.579(1)	5.137(2)	**2.587(1)**

(O··Na1··O)moy = 88.96 | ID(O··Na1··O) = 0.0912 | θ_{max}-θ_{moy} = 22.41 | θ_{moy}-θ_{min} = 13.78

Na(2)O$_6$

Na2	O10^{x}	O2	O12^{ii}	O6^{vii}	O7^{ix}	O5^{vi}
O10^{x}	**2.365(2)**	75.30(4)	157.95(5)	88.10(5)	80.97(4)	110.03(4)
O2	2.890(3)	**2.366(1)**	88.03(5)	157.99(5)	110.01(4)	80.92(3)
O12^{ii}	4.680(1)	3.314(1)	**2.403(2)**	111.32(3)	91.59(4)	80.77(3)
O6^{vii}	3.315(1)	4.681(2)	3.969(1)	**2.403(2)**	80.83(4)	91.62(4)
O7^{ix}	3.219(1)	4.058(1)	3.578(4)	3.237(3)	**2.585(2)**	166.58(3)
O5^{vi}	4.060(3)	3.219(2)	3.236(2)	3.581(2)	5.137(3)	**2.587(2)**

(O··Na2··O)moy = 90.79 | ID(O··Na2··O) = 0.1113 | θ_{max}-θ_{moy} = 20.53 | θ_{moy}-θ_{min} = 10.02

Te(1)O$_6$

Te1	O7^{v}	O7	O7^{iv}	O5^{v}	O5^{iv}	O5
O7^{v}	**1.911(1)**	92.38(5)	92.38(5)	174.36(4)	83.73(4)	91.87(4)
O7	2.758(2)	**1.911(1)**	92.38(5)	83.73(4)	91.87(4)	174.36(4)
O7^{iv}	2.758(2)	2.758(2)	**1.911(1)**	91.87(4)	174.36(4)	83.73(4)
O5^{v}	3.818(2)	2.552(1)	2.747(2)	**1.912(1)**	92.28(5)	92.28(5)
O5^{iv}	2.552(1)	2.747(1)	3.818(2)	2.757(1)	**1.912(1)**	92.28(5)
O5	2.747(1)	3.818(2)	2.552(1)	2.757(1)	2.757(1)	**1.912(1)**

Te(2)O$_6$

Te2	O9^{iv}	O9	O9^{v}	O3	O3^{v}	O3^{iv}
O9^{iv}	**1.911(1)**	92.34(5)	92.34(5)	83.73(4)	91.87(4)	174.36(4)
O9	2.757(2)	**1.911(1)**	92.34(5)	174.36(4)	83.73(4)	91.87(4)
O9^{v}	2.757(2)	2.757(2)	**1.911(1)**	91.87(4)	174.36(4)	83.73(4)
O3	2.551(1)	3.818(1)	2.746(2)	**1.912(1)**	92.32(5)	92.32(5)
O3^{v}	2.746(2)	2.551(1)	3.818(1)	2.757(2)	**1.912(1)**	92.32(5)
O3^{iv}	3.818(1)	2.746(2)	2.551(1)	2.757(2)	2.757(2)	**1.912(1)**

P(1)O$_4$

P1	O2	O8^{ii}	O8^{i}	O8
O2	**1.496(1)**	112.05(4)	112.05(4)	112.05(4)
O8^{ii}	2.532(1)	**1.556(2)**	106.77(4)	106.77(4)
O8^{i}	2.532(1)	2.499(1)	**1.556(2)**	106.77(4)
O8	2.532(1)	2.499(1)	2.499(1)	**1.556(2)**

ID(P1···O) = 0.0146 | D$_{max}$-D$_{min}$ = 0.060 | θ_{max}-θ_{min} = 5.28

P(2)O$_4$

P2	O4	O6	O6^{iii}	O6^{viii}
O4	**1.500(1)**	112.07(4)	112.07(4)	112.07(4)
O6	2.534(2)	**1.556(1)**	106.76(4)	106.76(4)
O6^{iii}	2.534(2)	2.498(1)	**1.556(1)**	106.76(4)
O6^{viii}	2.534(2)	2.498(1)	2.498(1)	**1.556(1)**

ID(P2···O) = 0.0136 | D$_{max}$-D$_{min}$ = 0.056 | θ_{max}-θ_{min} = 5.31

P(3)O$_4$

P3	O11	O12^{viii}	O12^{iii}	O12
O11	**1.498(1)**	112.09(4)	112.09(4)	112.09(4)
O12^{viii}	2.534(2)	**1.558(1)**	106.73(5)	106.73(5)
O12^{iii}	2.534(2)	2.500(1)	**1.558(1)**	106.73(5)
O12	2.534(2)	2.500(1)	2.500(1)	**1.558(1)**

ID(P3···O) = 0.0146 | D$_{max}$-D$_{min}$ = 0.060 | θ_{max}-θ_{min} = 5.36

P(4)O$_4$

P4	O10	O1^{i}	O1^{ii}	O1
O10	**1.494(2)**	112.12(3)	112.12(3)	112.12(3)
O1^{i}	2.533(1)	**1.558(1)**	106.70(4)	106.70(4)
O1^{ii}	2.533(1)	2.500(2)	**1.558(1)**	106.70(4)
O1	2.533(1)	2.500(2)	2.500(2)	**1.558(1)**

ID(P4···O) = 0.0154 | D$_{max}$-D$_{min}$ = 0.064 | θ_{max}-θ_{min} = 5.42

Symmetry codes :

(i) -y+1, x-y+1, z ; (ii) -x+y, -x+1, z ; (iii) -x+y+1, -x+1, z ; (iv) -y, x-y, z ; (v) -x+y, -x, z ; (vi) -y, x-y, z+1 ; (vii) x-1, y, z+1 ; (viii) -y+1, x-y, z ; (ix) -y, x-y+1, z+1 ; (x) x, y, z+1 ;
(xi) x, y, z-1 ; (xii) x+1, y, z-1 ; (xiii) -y+1, x-y+1, z-1 ; (xiv) -x+y-1, -x, z-1 ; (xv) -x+y, -x, z-1 ; (xvi) -x+y, -x+1, z-1.

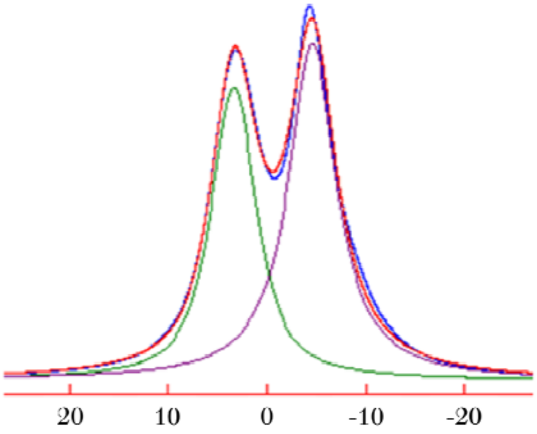

Figure 1. ^{23}Na MAS NMR spectrum of the sample (nf=10KHz)

to (4.8-44) and collected 12247 reflections in the hkl ranges $-15 \leq h \leq 12$, $-4 \leq k \leq 14$ and $-21 \leq l \leq 20$.
The examination of the hkl reflections shows the presence of some 00l (l = 2n) reflections at higher l values with very weak intensities, for example (0020).

When we ignored these reflections with weak intensities and we tried to solve the structure in the hexagonal system with the $P6_322$ space group we were unable to do so. During refinement we could not localize all atoms. The atomic positions remained unstable and the reliability factors R and R_W did not exceed 6.8 % and 15 %, respectively.

The structure was however solved by the Patterson method using SHELX-S 86 [22] in the trigonal system with the P3 space group. The refinement calculation was performed with the SHELX-L 93-computer program [23]. The obtained solution permitted us to localize the positions of the Te and P atoms. Positions of the Na and O atoms were located after subsequent Fourier series analysis. The reliability factors R and R_W fell to 2.5 % and 6 %, respectively.

As the structure was solved in a non-centrosymmetric space group, the determination of the Flack absolute structure parameter x [24, 25] was a good criterion to confirm the choice of the space group. Its refined value is here $x = 0.02\ (2) \approx 0$.
The details of data collection and refinement for the title compound are summarized in **Table 1**. The main geometrical features, bond distances, angles and the ID Baur [26] Distortion are reported in **Table 2.**

Electrical measurement

A polycrystalline pellet, 8 mm in diameter and 1.2 mm in thickness, was obtained at room temperature under pressure. Electrical properties were determined by impedance method using a Novo Control apparatus working with an automatic bridge interfaced to compatible microcomputer. The frequency range used was 1Hz to 1MHz. The temperature was measured with a chromel-alumel thermocouple close to the sample and data were collected in air in the temperature range 60-140°C.

Results and Discussion

NMR results

The ^{23}Na and ^{31}P NMR spectroscopies are very useful tools in determining the numbers of non-equivalent nucleus sites and their relative occupancies. Further information may be gained from the anisotropic NMR parameters characterizing the ^{23}Na quadrupole coupling interaction (*i.e.* χ_Q and η_Q) and the ^{31}P chemical shielding anisotropy tensors (*i.e.* δ_σ and η_σ) in addition to the ^{23}Na and ^{31}P isotropic chemical shifts. The ^{23}Na MAS NMR spectrum of the sample is shown in **figure 1**, which clearly demonstrates the existence of two distinct sodium sites. The values of quadrupole interaction parameters obtained from the ^{23}Na MAS NMR are summarized in **table 3**. There is a significant difference between the values of η and χ for the two sites of sodium nucleus. This result is undoubtedly related to crystallographic parameters, providing a clear discrimination between the two sites and distinguishing the structure here reported from that of Averbuch-Pouchot [19].

The ^{31}P spectrum for a sample rotating at the magic angle with 10 KHz frequency is shown in **figure 2**. A simulation of the spectrum displays four ^{31}P resonance lines at 1.6, 2.8, 3.2 and 3.8 ppm in similar abundance (**table 3**). This suggests the existence of four crystallographically inequivalent phosphorus atoms in the materials. Using the iterative procedure of Herzfeld and Berger [27], we attempted to deduce the parameters of the chemical shift tensor: the isotropic, the chemical shift anisotropy and the asymmetry parameter (**table 3**).

Table 3. The values of quadrupole interaction parameters obtained from ^{23}Na and ^{31}P MAS NMR and also chemical shift tensor information for ^{31}P RMN spectrum.

Site	%	δ_{iso} (ppm)	δ_{cs} (ppm)	G/L	χ (KHz)	η	δ_{11}	δ_{22}	δ_{33}
Na1	45	3.4	-	0.2	0.2	0.6	-	-	-
Na2	55	-4.6	-	0.0	0.4	0.4	-	-	-
P1	25	1.6	-16.5	0.4	-	0.0	9.8	9.8	-14.9
P2	23	3.8	-24.7	0.2	-	0.7	24.6	7.5	-20.9
P3	26	3.2	41.2	0.4	-	0.5	-28.8	-6.1	44.4
P4	26	2.8	41.2	0.6	-	0.6	-30.2	-5.5	44.0

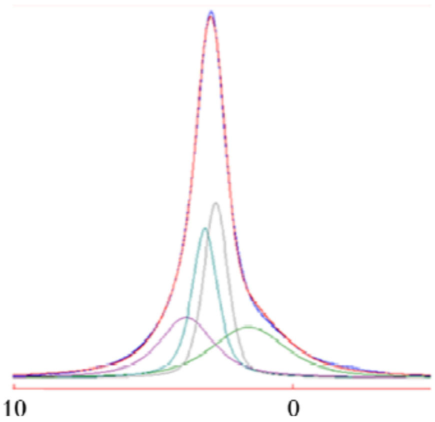

Figure 2. ^{31}**P MAS NMR spectrum of the sample (nf=10KHz)**

The range of isotropic values at about 0-5 ppm lies in the $Q^{(0)}$ domain indicating phosphorus without bridging oxygen ions.

Structure description

A projection of the NaPTe structure along the [100] direction is depicted in **figure 3**. The structure is being built by no pure sheets of the $Te(OH)_6$ octahedra parallel to (001), at 1/4 and 3/4 apart alternating with sheets of pure PO_4 tetrahedra at 0 and 1/2 apart. The Na^+ cations have an octahedral coordination and occupy the large cavities formed by the TeO_6 octahedra sheet.

The main difference between the two sheets of the TeO_6 octahedra is the two different sodium sites. In fact, the first sheet z = 1/4 is formed by $Te(1)O_6$ octahedra, each of which is surrounded by six octahedra of Na(1). The second sheet z = 3/4 is formed by octahedra of $Te(2)O_6$, each of which is surrounded by six octahedra of Na(2).

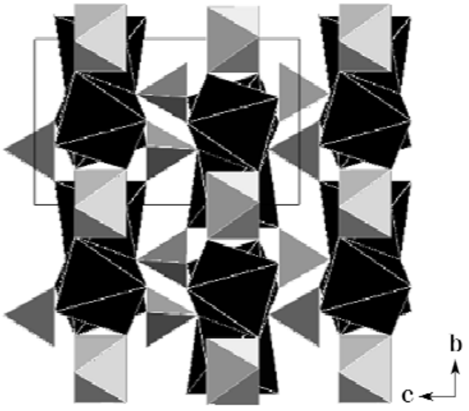

Figure 3. [100] view of the structure of $Na_2HPO_4NaH_2PO_4Te(OH)_6$. The small medium grey octahedra represent $Te(OH)_6$ and the black ones represent Na cation environments. PO_4 anions are represented by grey tetrahedra.

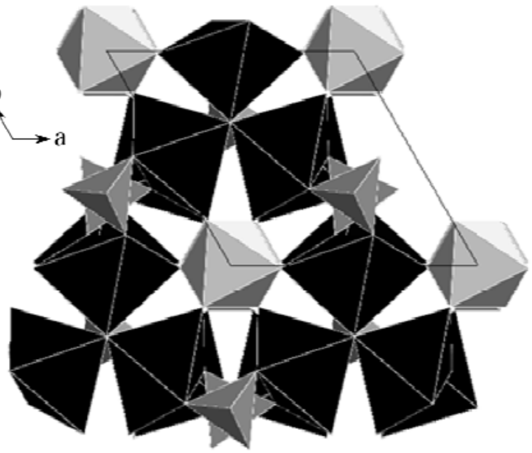

Figure 4. Projection of $Na_2HPO_4NaH_2PO_4Te(OH)_6$ crystal structure on the ab plane which shows NaO_6, TeO_6 and PO_4 environments.

The PO_4 tetrahedra can be described as belonging to the same sheet directions, but alternating with the $Te(OH)_6$ ones. The PO_4 tetrahedra are arranged in two membered groups; in each group they have opposite directions.

Geometry and coordination of NaO_6 anions

All NaO_6 octahedra are gathered in three membered groups around an A_3 axe and sharing one bridging oxygen atom. For the Na(1) atom, the octahedra base is formed by O8–O1–O4–O11. The O9 and O3 non-basal oxygen atoms are shared with two $Te(1)O_6$ octahedra; O4 and O11 form a common edge linking the NaO_6 group. The same coordination is described for the Na(2). The base of this octahedron is build by O22–O32–O11–O41. The non-basal oxygen atoms (O1 and OT21) are shared with two $Te(2)O_6$ octahedra. The common edge for the NaO_6 group is formed by O11 and O41.

For both sodium sites, the Na···O distances from the basal oxygen atoms are all relatively short and lie in the range 2.364(2)–2.403(1) Å, and all O···Na···O angles involving the basal oxygen atoms lie in the range 75.3(1)–110(1)°. As a consequence, the four basal oxygen atoms form an approximately pseudo-square arrangement. The Na···O distances from the non-basal oxygen atoms are typically longer than those from the basal ones, and are about 2.586(1) Å. In addition, $Na(1)O_6$ and $Na(2)O_6$ have relatively the same edge values and consequently the same Baur distortion indices (ID) [26]: ID(Na···O) = 0.0368, ID(O···O) = 0.1465.

The main differences in local structure between the two sodium sites concern the angles; especially the O3···Na(1)···O11 angle of 88.09(5)° in the first site corresponding to the O7···Na(2)···O2 angle of

110.01(4)° in the second site, which suggests a distortion of the angle in the second site. This distortion has consequently yielded slightly different values in the other angles compared with the values of the corresponding angles from the first site. This finding can explain the difference between the ID(O···Na···O) indices for the two sites; 0.091 for the Na(1) site and 0.111 for the Na(2) site.

Geometry and coordination of TeO_6 anions

In the title compound NaPTe, the Te atoms occupy two special positions with the obtained Te–O distances about 1.912(1) Å. For the two kinds of Te, the O–Te–O angle values vary from 83.73(4)° to 92.38(5)°. These values are different from those observed in the previously described compound [19]. Indeed, in the latter, the six obtained Te–O distances are equal to 1.923(1) Å with O–Te–O angles between 84.19° and 92.22°.

Geometry and coordination of PO_4 groups

The asymmetric unit presents four unequivalent phosphorus sites: All PO_4 tetrahedra have C_{3V} punctual symmetry. The shortest P–O band, looked along the A_3 axis, varies from 1.494(2) to 1.500(1) Å. This variation causes a slight distortion ID(P–O) in the four sites. The other P–O bands have almost the same distance value (1.557(1) Å), which remains the same for all the sites. Each PO_4 tetrahedron has three O–P–O angles of 112.09(4)° and three other angles of 106.73(4)°.

Impedance analysis

Figure 5 shows the plot of imaginary part (*Z″*) versus real part (*Z′*) of complex impedance taken over the frequency range 1Hz - 1MHz at different temperatures 60°C ≤ T ≤ 135°C. All the semicircles of the compound exhibit some depression instead of a semicircle centred on the real axis. Such behaviour is indicative of non-Debye type of relaxation [28].

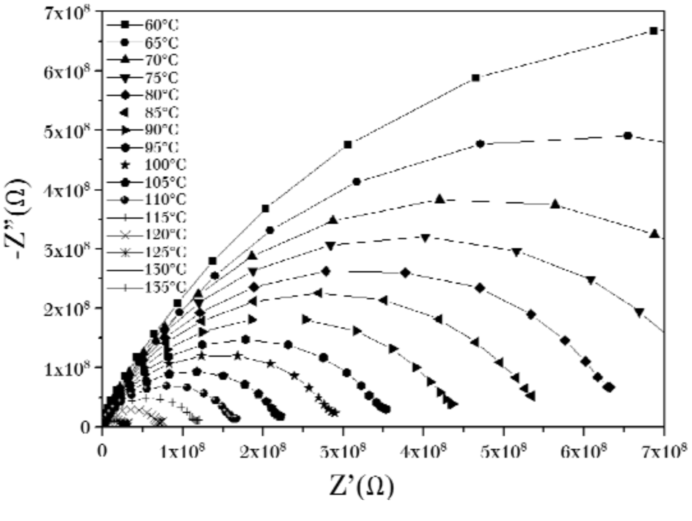

Figure 5. Complex impedance plots of Z”(Ω) vs. Z’(Ω) at various temperatures for $Na_2HPO_4NaH_2PO_4Te(OH)_6$ compound.

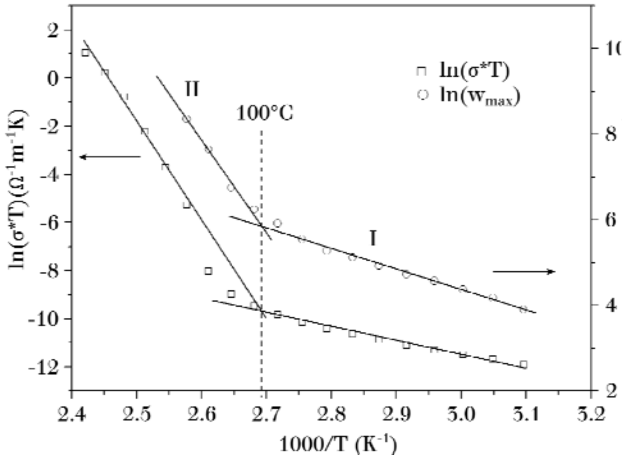

Figure 6. Temperature dependence of Ln(σT) and Ln(W_{max}) versus reciprocal temperature for $Na_2HPO_4NaH_2PO_4Te(OH)_6$ compound.

The bulk ohmic resistance relative to each experimental temperature is deduced from complex impedance diagrams, it is the interception Z_0 on the real axis of the zero phase angle of extrapolation in the lower frequency curve. The conductivity is obtained from Z_0 by means of the relation: $\sigma = e/SZ_0$, where e and S represent the thickness and the area of the sample, respectively. The temperature dependence of the conductivity is given in **figure 6** for the compound as a plot of ln(σT) versus reciprocal temperature. The conductivity plot exhibits two parts with a transition at about 370K, which characterizes the crossing of conductivity. In consequence, the diagram exhibits two regions. In these two regions, the evolution of the conductivity σ obeys the Arrhenius-type relation: $\sigma T=\sigma_0 \exp(-E_a/KT)$. The activation energies above and below the transition are, respectively, $\Delta E_1=0.42$ eV and $\Delta E_2=3.54$ eV. On the other hand, the conductivity increases from $\sigma T=5.34*10^{-5}\ \Omega^{-1}m^{-1}K$ at 95°C to $\sigma T=5.09*10^{-3}\ K\Omega^{-1}m^{-1}$ at 115°C. In spite of all the results indicated above, the high temperature phase transition at about 100°C in the NaPTe compound can be interpreted as an ionic-protonic one.

An analysis of the ion conductivity relaxation process in the compound has been undertaken in the study of imaginary part of complex impedance versus the frequency.

Figure 7 shows the variation of imaginary (Z”) parts of impedance with frequency at various temperatures. All the curves merge in high-frequency region (>10^4 Hz), and then Z” becomes independent of frequency. Moreover, the variation of Z” with frequency at various temperatures reveals that Z” values reach a maximum (Z”max), which shifts to higher frequencies with increasing temperature. Such behavior indicates the presence of relaxation phenomenon in the system.

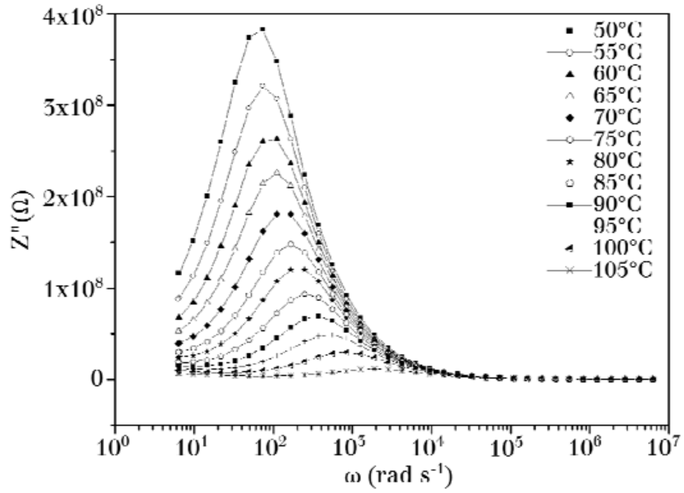

Figure 7. Variation of imaginary parts (Z”) of impedance as a function of frequency for some representative temperature.

Figure 6 shows also the variation of ln(W_{max}) with the inverse of absolute temperature (10^3/T), where W_{max} is a particular frequency in which Z” occupies a maximum value. This plot is explained by Arrhenius-type relation:

$$W_{max} = Bexp\left(\frac{E_a}{K_B T}\right)$$

where B is the pre-exponential factor, K_B the Boltzmann’s constant and E_a is the thermal activation energy for the ion migration. The change in the slope of the linear curve is detected around 100°C. The value of the activation energy determined in region I is 0.45 eV. This value is similar to the activation energy determined by the conductivity analysis. This result suggests that the ion transport in polycrystalline and single crystal are probably due to a hopping mechanism [29].

Electrical conductivity analysis

The frequency dependence of AC conductivity, $\sigma_{ac}(\omega)$, at various temperatures for the NaPTe material is shown in **figure 8**. The AC conductivity increases with increase of the frequency showing an ω^n characteristic law. The phenomenon of the conductivity dispersion in solids is generally analysed using Jonscher's law: $\sigma_{ac} = \sigma_{dc} + Aw^n$, where σ_{dc} is the direct current conductivity, A is a temperature-dependent parameter, and n is the dimensionless frequency exponent parameter in the range of $0 \leq n \leq 1$ [30, 31, 32, 33]. The exponent n represents the degree of interaction between mobile ions with the lattices around them, and the prefactor exponent A determines the strength of polarizability. Typical fit of the above equation to the experimental analysis data suggests that $\sigma_{ac}(\omega)$ obeyed Jonscher's law (**fig.8**). The high frequency dispersion is attributed to AC conductivity, whereas the frequency-independent plateau region corresponds to DC conductivity of the material. The values of n for an ideal Debye dielectric and ideal ionic-type crystal are 1 and 0, respectively **[34]**. The movement or hopping of the charged carrier is influenced by its neighbourhood, and the exponent n is a measure of the degree of interaction.

In order to explain the behaviour of σ with both frequency and temperature, different theoretical models have been proposed to correlate the conduction mechanism of AC conductivity with n(T) behaviour [35]. According to quantum mechanical tunneling model [32, 36, 37], the exponent n is temperature independent. The large overlapping

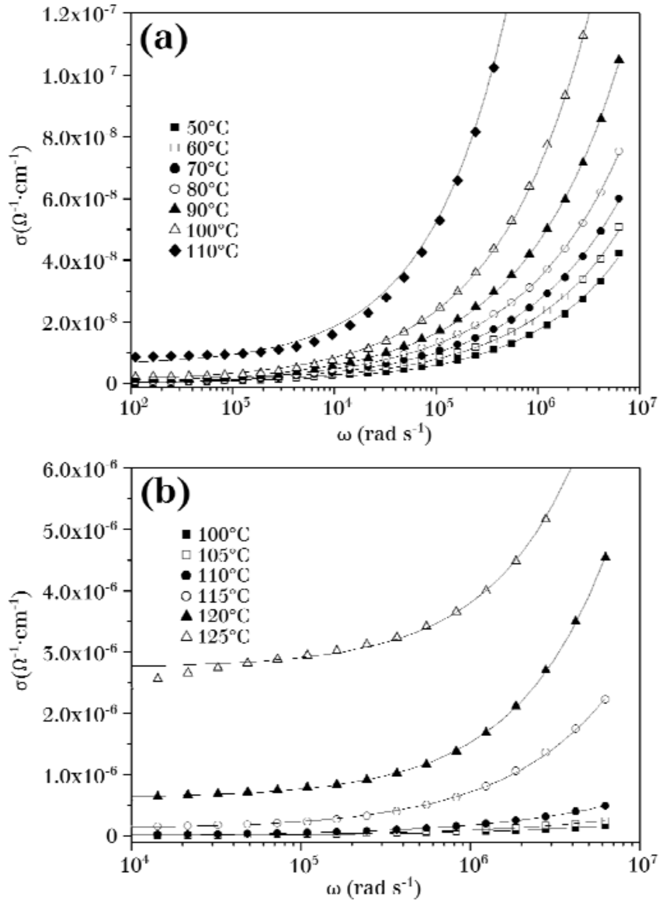

Figure 8. Dependence of AC conductivity $\sigma_{ac}(\omega)$ on angular frequency at different temperature for $Na_2HPO_4NaH_2PO_4Te(OH)_6$

polaron model [37] predicted that n decreases with increasing temperature up to a certain temperature degree, after which, it begins to increase with further rise in temperature. The small polaron tunneling model and the classical hopping model over a barrier separating two sites [38] predicted that n decreases with increasing the temperature.

The temperature dependence on the fitted frequency exponent n and the pre-exponential factor A are shown in **figure 9**. In the temperature range below 100°C, the value of n decreases with increasing temperature, after which it increases with increasing temperature. Comparing our results of n(T) with the above mentioned models, it can be concluded that the large overlapping polaron model is the most probable conduction mechanism for the NaPTe material.

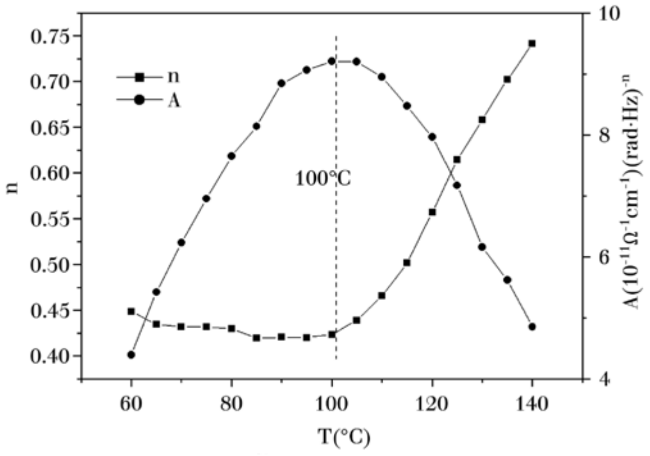

Figure 9. Thermal variation of the fitted power exponent n and the pre-exponential parameter A using Jonscher's law for $Na_2HPO_4NaH_2PO_4Te(OH)_6$

Conclusion

The structure of the $Na_2HPO_4NaH_2PO_4Te(OH)_6$ has been determined on a single crystal. The structure shows that the compound crystallizes in a trigonal system with a P3 space group. The examination of the local environments for the Na and P atoms by MAS NMR reveals the presence of two sites of Na and four sites of P. These features distinguish the structure reported here from that reported by Averbuch-Pouchot [19]. The main characteristic of the structure here reported is the presence of two different and independent anionic groups connected by hydrogen bonds. The $Te(OH)_6$ octahedra belong to a number of sheets perpendicular to the c axis alternating with sheets of PO_4 tetrahedra also perpendicular to the c axis. The Na^+ cations are coordinated by six oxygen atoms and alternating with the $Te(OH)_6$ octahedra in the same sheet. Electrical study shows a strong jump in the conductivity at 370 K. The AC conductivity showed a variation with frequency, and it was found to obey Jonscher's universal power law at different temperatures with n varying from 0.45 to 0.75. The conduction process in the AC conductivity is explained by the large overlapping polaron model up to 100°C.

References

1. Zilber R, Durif A, Averbuch-Pouchout MT, (1980) Structure of potassium sulphate tellurate: $K_2SO_4Te(OH)_6$. Acta Crystallographica B (36): 2743-2745.
2. Dammak M, Khemakhem H, Mhiri T, Kolsi AW, Daoud A, (1999) Structural and Vibrational Study of $K_2SeO_4Te(OH)_6$ Material. Journal of Solid State Chemistry (145): 612-618.
3. Dammak M, Khemakhem H, Mhiri T, Kolsi AW, Daoud A, (1998) Structure and characterization of a mixed crystal $Rb_2SO_4Te(OH)_6$. Journal of Alloys and Compounds (280): 107-113.
4. Abdelhedi M, Dammak M, Cousson A, Kolsi AW, (2005) Structural, calorimetric and conductivity study of the new mixed solution $Rb_2(SO_4)_{0.5}(SeO_4)_{0.5}Te(OH)_6$. Journal of Alloys and Compounds (398): 55-61.
5. Litaiem H, Dammak M, Mhiri T, Cousson A, (2005) Structural, conductivity and dielectric studies in $(NH_4)_2SeO_4Te(OH)_6$. Journal of Alloys and Compounds (396): 34-39.
6. Guillot Gauthier S, Peuzin JC, Olivier M, Rolland G, (1984) Monoclinic telluric acid ammonium phosphate (TAAP) a new ferroelectric compound III dielectric and related properties. Ferroelectrics (52): 293-306.
7. Merinov BV, Jones DJ, Rozière J, Mhiri T, (1994) Structure of mixed alkali metal sulfate proton conductors: Dynamically disordered hydrogen bond network in $Cs_{1.5}Li_{1.5}H(SO_4)_2$. Solid State Ionics (69): 53-58.
8. Dammak M, Khemakhem H, Mhiri T, (2001) Superprotonic conduction and ferroelectricity in addition cesium sulfate tellurate $Cs_2SO_4Te(OH)_6$. Journal of Physics and Chemistry of Solids (62): 2069-2074.
9. Chabchoub N, Khemakhem H, Gargouri M, (2003) Ferroelectricity and superionic conduction in telluric sulfates MM'(SO4)Te(OH)6 (M, M'=K, Rb and Cs). Journal of Alloys and Compounds (359): 84-90.
10. Schmidt VH, Bohannan G, Arbogast D, Tuthill G, (2000) Domain wall freezing in KDP-type ferroelectrics. Journal of Physics and Chemistry of Solids (61): 283-289.
11. Jong-Ho Park & Byung-Chun Choi, (2003) Electrical conductivity and impedance characteristics of RbH_2PO_4 crystal above room temperature. Materials Letters (57): 2162-2167.
12. Ponomareva VG & Shutova ES, (2007) High-temperature behavior of CsH_2PO_4 and CsH_2PO_4–SiO_2 composites. Solid State Ionics (178): 729-734.
13. Yu-ki Taninouchi, Tetsuya Uda, Yasuhiro Awakura, (2008) Dehydration of CsH_2PO_4 at temperatures higher than 260 °C and the ionic conductivity of liquid product. Solid State Ionics (178): 1648-1653.
14. Ishikawa A, Maekawa H, Yamamura T, Kawakita Y, Shibata K, Kawai M, (2008) Proton dynamics of CsH_2PO_4

studied by quasi-elastic neutron scattering and PFG-NMR. Solid State Ionics (179): 2345-2349.

15. Averbuch-Pouchout MT, Durif A, Guitel JC, (1979) Structure crystalline d'un phosphate tellurate de rubidium: $Te(OH)_6Rb_2HPO_4RbH_2PO_4$. Materials Research Bulletin (14): 1219-1223.
16. Averbuch-Pouchout MT, Durif A, Guitel JC, (1980) Crystal structures of two cesium phosphate tellurates : $Te(OH)_62CsH_2PO_4CsHPO_4$ and $Te(OH)_6Cs_2HPO_4$. Materials Research Bulletin (15): 387-395.
17. Averbuch-Pouchout MT, Durif A, (1981) Crystal data for two new phosphate tellurates : $Te(OH)_62TlH_2PO_4TlHPO_4$ and $Te(OH)_62TlH_2PO_4$ crystal structure of $Te(OH)_62TlH_2PO_4$. Materials Research Bulletin (16): 71-76.
18. Kikuta T, Hamatake D, Yamazaki T, Nakatani N, (2005) Crystal Structure of Telluric Acid Ammonium Phosphate (TAAP) in the Paraelectric Phase. Journal- Korean Physical Society (46): 211-216.
19. Averbuch-Pouchout M.T., (1980) Structure d'un phosphate tellurate de sodium: $Te(OH)_6.Na_2HPO_4.NaH_2PO_4$. Acta Crystallographica B (36): 2405-2406.
20. Massiot D, Fayon F, Capron M, King I, Le Calvé S, Alonso B, Durand J-O, Bujoli B, Gan Z, Hoatson G, (2002) Modelling one and two-dimensional solid-state NMR spectra. Magnetic Resonance in Chemistry (40): 70-76.
21. Sheldrick G.M, (2004) SADABS. Germany: University of Göttingen.
22. Sheldrick G.M, (1990) SHELX-S 86. Germany: University of Göttingen.
23. Sheldrick G.M, (1993) SHELX-L 93. Germany: University of Göttingen.
24. Flack HD, (1983) On enantiomorph-polarity estimation. Acta Crystallography A (39): 876-881.
25. Bernardinelli G & Flack HD, (1985) Least-squares absolute-structure refinement. Practical experience and ancillary calculations. Acta Crystallography A (41): 500-511.
26. Baur WH, (1974) The geometry of polyhedral distortions. Predictive relationships for the phosphate group. Acta Crystallographica B (30): 1195-1215.
27. Herzfeld J, Berger AEJ, (1980) Sideband intensities in NMR spectra of samples spinning at the magic angle. Journal of Chemical Physics (73): 6021-6031.
28. Sena S, Choudhary RNP, Pramanik P, (2007) Structural and electrical properties of Ca^{2+}-modified PZT electroceramics. Physica B (387): 56-62.
29. Réau JM, Rossignol S, Tanguy B, Rojo JM, Herrero P, Rojas RM, Sanz J, (1994) conductivity relaxation parameters of some Ag^+ conducting tellurite glasses containing AgI or $(AgI)_{0.75}(TlI)_{0.25}$ eutectic mixture. Solid State Ionics (74): 65-73.
30. Jonscher AK, (1983) Dielectric relaxation in solids. London: Chelsea Dielectrics.
31. Hill RM, Jonscher AK, (1979) DC and AC conductivity in hopping electronic systems. Journal of Non-Crystalline Solids (32): 53-69.
32. Mott NF, Davis EA, (1979) Electronic processes in non-crystalline materials. Oxford: Clarendon Press 2nd ed.
33. Chen RH, Chang RY, Shern SC, (2002) Dielectric and AC ionic conductivity investigations in $K_3H(Se0_4)_2$ single crystal. Journal of Physics and Chemistry of Solids (63): 2069-2077.
34. Chen RH, Yen C, Shern CS, Fukami T, (2006) Impedance spectroscopy and dielectric analysis in KH_2PO_4 single crystal. Solid State Ionics (177): 2857-2864.
35. Elliott SR, (1977) A theory of AC conduction in chalcogenide glasses, Philosophical Magazine (36): 1291-1304.
36. Böttger H, Bryksin VV, (1976) Hopping conductivity in ordered and disordered solids. physica status solidi B (78): 415-451.
37. Long AR, (1982) Frequency-dependent loss in amorphous semiconductors. Advances in Physics (31): 553-637.
38. Elliott SR, (1987) AC conduction in amorphous chalcogenide and pnictide semiconductors. Advances in Physics (36): 135-217.